A new model for the growth of basaltic shields based on deformation of Fernandina volcano, Galápagos Islands

Marco Bagnardi [a,*], Falk Amelung [a], Michael P. Poland [b]

[a] Division of Marine Geology and Geophysics, Rosenstiel School of Marine and Atmospheric Science, University of Miami, 4600 Rickenbacker Cswy, Miami, FL 33149, USA
[b] U.S. Geological Survey, Hawaiian Volcano Observatory, PO box 51, Hawaii National Park, HI 96718-0051, USA

ABSTRACT

Space-geodetic measurements of surface deformation produced by the most recent eruptions at Fernandina – the most frequently erupting volcano in the Galápagos Archipelago – reveal that all have initiated with the intrusion of subhorizontal sills from a shallow magma reservoir. This includes eruptions from fissures that are oriented both radially and circumferentially with respect to the summit caldera. A Synthetic Aperture Radar (SAR) image acquired 1–2 h before the start of a radial fissure eruption in 2009 captures one of these sills in the midst of its propagation toward the surface. Galápagos eruptive fissures of all orientations have previously been presumed to be fed by vertical dikes, and this assumption has guided models of the origin of the eruptive fissure geometry and overall development of the volcanoes. Our findings allow us to reinterpret the internal structure and evolution of Galápagos volcanoes and of similar basaltic shields. Furthermore, we note that stress changes generated by the emplacement of subhorizontal sills feeding one type of eruption may control the geometry of subsequent eruptive fissures. Specifically, circumferential fissures tend to open within areas uplifted by sill intrusions that initiated previous radial fissure eruptions. This mechanism provides a possible explanation for the pattern of eruptive fissures that characterizes all the western Galápagos volcanoes, as well as the alternation between radial and circumferential fissure eruptions at Fernandina. The same model suggests that the next eruption of Fernandina will be from a circumferential fissure in the area uplifted by the 2009 sill intrusion, just southwest of the caldera rim.

© 2013 Elsevier B.V. All rights reserved.

1. Introduction

Current understanding of the construction and evolution of basaltic shield volcanoes is largely based on studies of Hawai'i. The great attention paid to Hawaiian volcanoes, particularly Kīlauea and Mauna Loa, is justified given their accessibility and long-term record of observation and instrumental monitoring (Kauahikaua and Poland, 2012). Intrusive/effusive activity at these locations often occurs along narrow radial rift zones that are a product of magmatic and tectonic processes within the volcanic edifices (Dieterich, 1988; Fiske and Jackson, 1972; Tilling and Dvorak, 1993). Both geologic studies of eroded volcanoes (Walker, 1987) and geological/geophysical monitoring of active volcanoes (Pollard et al., 1983) indicate that intrusions within these rift zones occur as subvertical dikes, even proximal to the summit region. Such a conceptual model, however, represents an end member that is not necessarily representative of basaltic shields found elsewhere

on Earth and other planets (Batiza et al., 1984; Jaggar, 1931; Macdonald, 1948; Montési, 2001; Simkin, 1972).

Volcanoes of the western Galápagos Islands generally lack well-developed rift zones and are characterized instead by eruptive fissures oriented both circumferentially and radially with respect to the summit calderas (Chadwick and Howard, 1991, Fig. 1). These fissures are the surface expression of underlying subvolcanic intrusions that propagated from the magma reservoirs beneath the calderas. The conditions and mode of emplacement of these bodies is therefore fundamental to understanding the internal growth of the volcanoes.

The cause of the great difference between patterns of eruptive fissures at Hawaiian volcanoes versus those of the western Galápagos Islands has long been a source of speculation, especially given the similar intra-plate hotspot origin for the two archipelagos (Chadwick and Howard, 1991; Rowland and Munro, 1992). Motion of volcanic flanks has been tied to rift zone evolution in Hawai'i; however, flank instability in the Galápagos is not widespread, perhaps because the oceanic crust on which Galápagos volcanoes grow is young and lacks the sediment cover that may act to promote flank motion at other locations (Dieterich, 1988; Nakamura, 1980). Sequential growth of volcanoes in Hawai'i has

* Corresponding author. Tel.: +1 808 967 8807; fax: +1 808 967 8890.
E-mail addresses: mbagnardi@rsmas.miami.edu (M. Bagnardi), famelung@rsmas.miami.edu (F. Amelung), mpoland@usgs.gov (M.P. Poland).

also been suggested to control rift zone geometry through buttressing of newer volcanoes against older ones (Dieterich, 1988; Fiske and Jackson, 1972), but the western Galápagos volcanoes formed concurrently, limiting the buttressing effect between adjacent volcanoes (Naumann et al., 2002; Rowland and Munro, 1992). Most previous studies have attempted to explain the Galápagos radial-circumferential fissure pattern as due to topographic effects (Munro and Rowland, 1996; Simkin 1984, 1972), a response to caldera collapse (Nordlie, 1973), or magma reservoir geometry (Chadwick and Dieterich, 1995). All proposed models, however, make the assumption that both radial and circumferential eruptive fissures in the Galápagos are fed by subvertical dikes.

Here, we study surface deformation of Fernandina (the most frequently erupting volcano in the Galápagos) associated with the 2009 eruption and reexamine displacements associated with two previous eruptions (in 1995 and 2005). Our findings lead us to propose a new model for the internal growth of Galápagos volcanoes, as well as other basaltic shields that do not follow the Hawaiian example. Moreover, we observe that circumferential fissures in 2005 opened within an area that was deformed during the previous radial fissure eruption in 1995. We investigate the relation between the two modes of eruption by calculating the stress changes generated by the intrusions that feed radial fissures. These models suggest that deformation associated with one eruption can be used to project the probable location and orientation of future eruptive fissures (e.g., Walter, 2008).

2. Fernandina volcano, Galápagos

The application of space-geodetic techniques, such as Interferometric Synthetic Aperture Radar (InSAR) (Amelung et al., 2000), has provided an unprecedented opportunity over the past 20 years to study the subsurface structure of active volcanoes (e.g., Baker and Amelung, 2012). At Fernandina, InSAR data spanning both eruptive and inter-eruptive time periods are the basis for models of the magma storage system of the volcano. Fernandina is characterized by at least two hydraulically connected magma reservoirs, at ∼1 km and ∼5 km b.s.l. (Bagnardi and Amelung, 2012; Chadwick et al., 2011; Geist et al., 2006a). The deeper reservoir appears to be the source of large sill-like intrusions in 2006 and 2007 that are indicated by broad uplift of the southern flank of the volcano (Bagnardi and Amelung, 2012), while the shallower reservoir primarily feeds summit and flank eruptions (Chadwick et al., 2011).

Among Galápagos volcanoes, Fernandina best represents the characteristic pattern of radial and circumferential eruptive fissures (Fig. 1). InSAR is particularly instructive with regard to the origin of the fissure pattern, since data span both circumferential (2005) and radial (1995 and 2009) fissure eruptions, as shown in Fig. 2. Jónsson et al. (1999), studied deformation associated with the 1995 radial fissure eruption (Fig. 1(b)) and modeled the displacement recorded in a five-year differential interferogram (from the ERS-1/2 satellites) as due to a NE-SW-trending dike with a gentle dip (34° from horizontal) to the SE (yellow rectangle in Fig. 2(a)). These results argued, for the first time, that dikes feeding radial fissure eruptions in the Galápagos may not be vertical.

Chadwick et al. (2011) found that Global Positioning System (GPS) and InSAR data spanning the May 2005 circumferential eruption (Fig. 1(b)) could be fit by a dike that is shaped like a concave shell (curving both vertically and horizontally). The dike was steeply dipping near the surface (∼60°) but more gently dipping at its origin at ∼1 km depth (<15°), where it intersects the shallower magma reservoir (yellow, orange and gray rectangles in Fig. 2(b)).
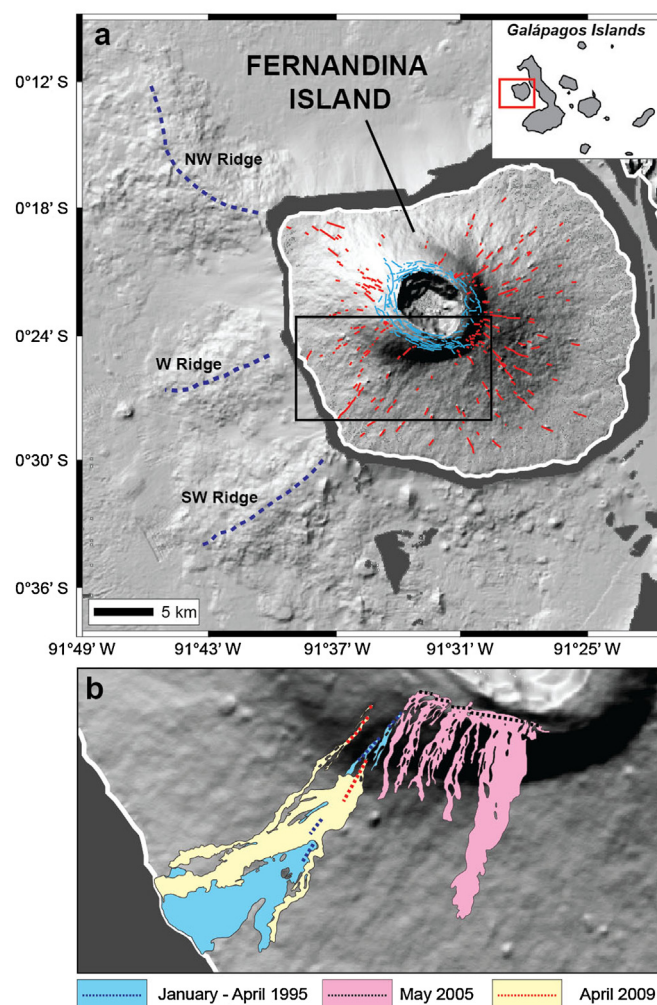

Fig. 1. Topography of Fernandina Island and its pattern of eruptive fissures. (a) Shaded relief map of Fernandina and surrounding ocean floor. Topography from SRTM data V4, bathymetry from NGDC-NOAA multi-beam data. In dark gray, areas where bathymetric data are not available. Solid lines represent circumferential (in blue) and radial (in red) eruptive fissures mapped by Chadwick and Howard (1991). Purple-dashed lines mark submarine ridges identified by Geist et al. (2006b). Inset: Location map of the Galápagos Islands. Black rectangle indicates area of part (b). (b) Close-up covering the location of the last three eruptions on Fernandina. Dashed lines mark eruptive fissures and filled polygons represent the surface covered by lava flows produced by each eruption. (For interpretation of the references to color in this figure legend, the reader is referred to the web version of this article.)

On 10 April 2009, between 23:30 and 00:00 local time, a new eruption started at Fernandina. The start time of the eruption is inferred from thermal data acquired by the Geostationary Operational Environmental Satellites (GOES; Fig. 3). No thermal anomalies were apparent prior to 23:30 on April 10 (April 11, 05:30 UTC), while high temperatures were recorded on the southwestern part of Fernandina Island in a subsequent image, acquired at 00:00 on April 11 (06:00 UTC). The eruption was characterized by three fissures that formed a left-stepping en echelon set between an elevation of 400 m and 1100 m a.s.l., oriented radially to the summit caldera and in the same sector of the volcano as the eruptions of 1995 and 2005 (Fig. 1(b)). Serendipitously, the Envisat satellite acquired a SAR image at 22:15 on April 10, 1–2 h before the opening of the first eruptive fissure, which captures the intrusion that fed the eruption in the midst of its emplacement. Subsequent SAR images span the entire duration of the eruption and allow a detailed analysis of the surface deformation associated with the event.
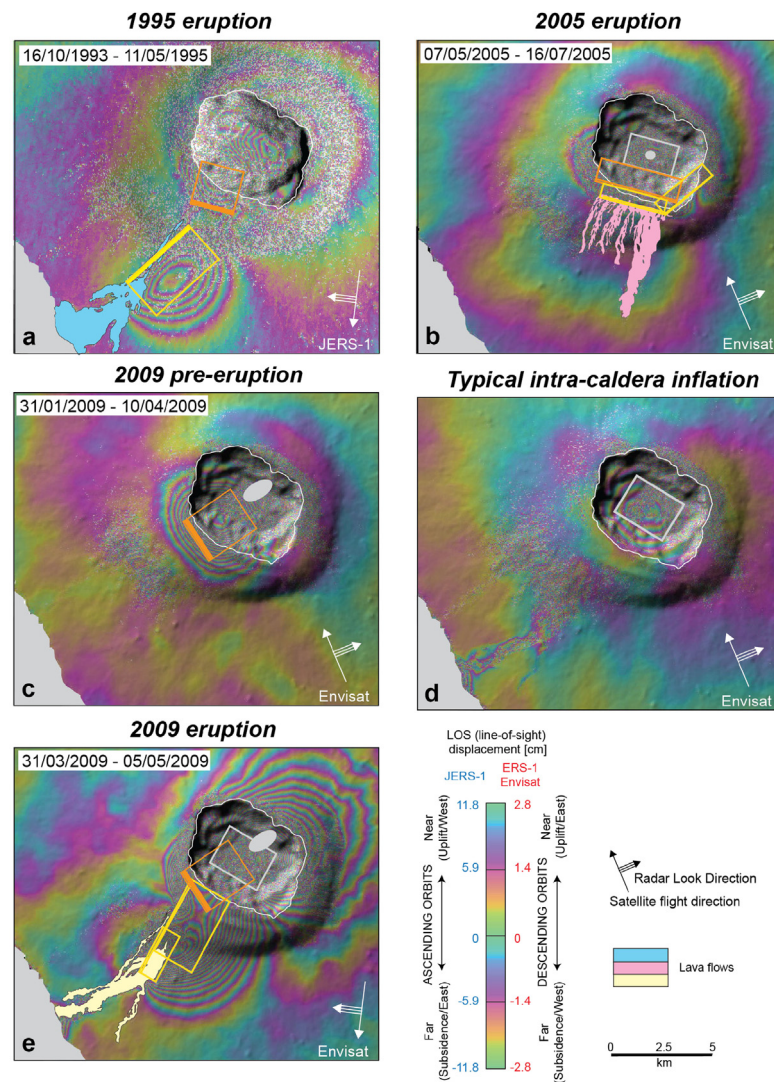
Fig. 2. Deformation at Fernandina. (a)–(e) Interferograms and modeling results. In gray are the deformation sources used to model magma reservoirs (rectangle: horizontal sill-like source at ∼1 km depth; ellipse and circle: deeper source at ∼5 km depth); yellow and orange rectangles outline planar sources used to model the intrusions feeding the eruptions (in orange, the subhorizontal segments). For inclined sources, the thicker line represents the shallower edge. (a) January–April 1995 eruption. (b) May 2005 eruption (model from Chadwick et al., 2011). (c) April 2009 pre-eruptive sill intrusion; interferogram formed using a SAR image acquired 1–2 h prior to the opening of the first eruptive fissure. (d) Typical pattern of deformation observed during several periods of intra-caldera uplift and due to the inflation of the ∼1-km-depth magma reservoir (Envisat interferogram, T61, ascending, 16/01/2010–14/08/2010, model from Bagnardi and Amelung (2012)). (e) Total displacement associated with the April 2009 eruption. (For interpretation of the references to color in this figure legend, the reader is referred to the web version of this article.)
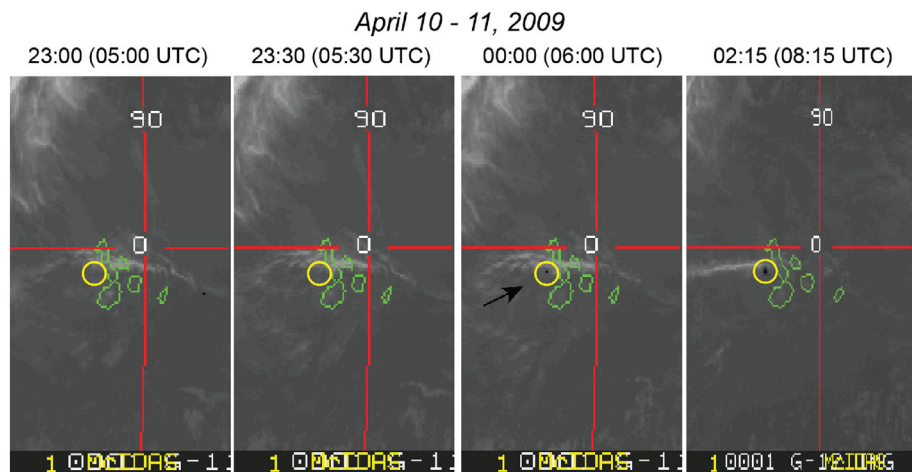

Fig. 3. GOES satellite thermal images showing the start time of the April 2009 eruption – Channel 2, 3.78–4.03 μm – yellow circle represents Fernandina volcano. The first appearance of a thermal anomaly (black pixel), representing the first evidence of a surface eruption, is in the 00:00 (06:00 UTC) image (black arrow). (For interpretation of the references to color in this figure legend, the reader is referred to the web version of this article.)

3. Data and methods

3.1. InSAR data processing and modeling

We used SAR data from the European Space Agency's ERS-1/2 and Envisat satellites and from the Japanese Aerospace Exploration Agency's JERS-1 satellite to construct interferograms showing deformation of Fernandina. All of the interferograms used in this study were processed using the Gamma SAR Processor and Interferometry software to focus the raw SAR images and the JPL/Caltech ROI_PAC SAR Software (Rosen et al., 2004) to form interferograms. We used precise DORIS orbits provided by the European Space Agency (ESA), and we removed the topographic contribution to the interferometric phase using a 90-m-resolution (resampled to 30 m) digital elevation model (DEM) generated by the NASA Shuttle Radar Topography Mission (SRTM; Farr et al., 2007). The interferograms were then phase-unwrapped using the *SNAPHU* algorithm (Chen and Zebker, 2001).

Deformation for both the 1995 and 2009 eruptions at Fernandina was modeled using analytical solutions for sources embedded in a homogeneous elastic half-space. For all models, we assumed a Poisson's ratio $\nu = 0.25$ and took into account the effect of topography on the surface deformation using the approach proposed by Williams and Wadge (1998). The optimal solutions and their probability density distributions were estimated through the nonlinear inversion of the InSAR data, which was performed using the Monte-Carlo-based Gibbs Sampling (GS) algorithm (Brooks and Frazer, 2005). The fit of the predicted deformation to the measured displacements was assessed using the normalized root-mean square error (*RMSE*) between observed and modeled interferograms. To reduce the number of data points (for which unit variance was assumed), a spatial averaging of full-resolution SAR interferograms was performed using a *Quadtree* algorithm (Jónsson et al., 2002).

3.2. Stress change modeling

Stress changes generated by the intrusion of planar magmatic bodies within the volcanic edifice were calculated using the Structural Mechanics module of the commercial Finite Element Modeling (FEM) program COMSOL Multiphysics. A three-dimensional model of the volcano (width, length and depth $100 \times 100 \times 100$ km) was constructed using topographic data from the SRTM DEM and assuming a linear elastic and isotropic body with typical elastic properties for basaltic extrusive and intrusive rocks (Poisson's ratio $\nu = 0.25$, shear modulus $\mu = 10$ GPa) and density $\rho = 2700$ kg/m^3 (Jónsson, 2009; Rubin and Pollard, 1987). The boundary conditions were set as free surface at the top and free to move horizontally and vertically at the bottom and sides of the model, respectively. We simulated the opening of planar bodies using inclined thin rectangular cavities with normal displacement (geometry, location and displacement inferred from the nonlinear inversion of the InSAR data). A convergence test was performed by moving the boundaries and changing the size of the mesh, which confirmed that those parameters do not significantly affect the numerical solutions.

To predict the probable location and orientation of future eruptive fissures, the stress changes caused by magmatic intrusions should be superimposed on the reference stress state within the volcanic edifice (Muller et al., 2001; Grosfils, 2007; Bistacchi et al., 2012); however, this reference stress is the result of multiple and complex factors (e.g., growth and evolution of the volcano, regional tectonics, etc.) and difficult to characterize. In our model, we made the assumption that, prior to each intrusion, the reference stress state is isotropic (or hydrostatic; e.g., Chadwick and Dieterich, 1995). Neither regional tectonic stress nor gravitational

load were applied, and we only examine the perturbation to a stress-free host rock generated by magmatic intrusions that fed eruptions.

4. Deformation observations and modeling results

4.1. April 2009 pre-eruptive intrusion

Differential interferograms formed using the Envisat SAR image acquired 1–2 h before the opening of the first eruptive fissure in 2009 show an area about 5.5 km in diameter near the southwestern rim of the summit caldera that uplifted by a maximum of 0.50 m in the satellite's line-of-sight (LOS) direction (Fig. 2(c)). The deformation clearly differs from the typical pattern of intra-caldera uplift that is caused by inflation of the shallower magma reservoir between eruptions, which is centered on, and generally confined within, the caldera (Fig. 2(d)). Interferograms formed using a SAR image acquired ∼13 h earlier (at 09:41 on April 10) do not show any evidence for similar displacements (see Fig. S1 in Supplementary Material), implying that the anomalous pre-eruptive deformation occurred sometime between 09:41 and 22:15 on April 10.

We modeled the LOS displacements from the immediate pre-eruptive interferogram (Envisat, track 61, beam mode IS2, ascending, 31/01/2009–10/04/2009) using a planar source with uniform opening and no dip- or strike-slip motion (Okada, 1985) and for which all source parameters were set free to float within geologically realistic bounds during the inversion. Weak subsidence around the uplifting area was modeled using a prolate spheroidal cavity (Yang et al., 1988), approximating Fernandina's deeper magma reservoir, with source parameters (except for the normalized pressure change) fixed to values from Bagnardi and Amelung (2012). The best-fitting model is a rectangular sill that dips gently (∼26°) toward the center of the volcano, originates below the caldera at ∼2.3 km b.s.l. and extends to ∼0.80 km b.s.l. (orange rectangle in Fig. 2(c)). Best-fitting planar source parameters are reported in Table S1 (Supplementary Material), and a comparison between the observed InSAR data, predicted LOS displacement, and the residual (difference between observed and predicted) is shown in Fig. 4.

4.2. April 2009 eruption – total displacement

The total displacement produced by the 2009 eruption was recorded by two nearly synchronous interferograms (each spanning 105 days) from the Envisat satellite, one from an ascending orbit (track 61, beam mode IS2) and one from a descending orbit (track 54, beam mode IS7). The measured displacements (Fig. 2(e)) reveal a pattern very similar to that associated with the previous eruption of a radial fissure, in 1995 (Fig. 2(a)). Broad, semi-circular, positive LOS displacement (uplift) is present on the east side of the eruptive fissures and is superimposed on negative displacement (subsidence) ranging across the entire volcanic edifice.

Given the complexity of the measured surface displacement, the use of multiple sources of deformation (five, in our preferred model) is necessary. Edifice-wide and intra-caldera subsidence is interpreted as deflation of the two subcaldera magma reservoirs (Bagnardi and Amelung, 2012) and was modeled using a prolate spheroidal cavity (Yang et al., 1988, source $r1$) and a planar source with uniform opening (Okada, 1985, source $r2$). For these two sources, all parameters that define position and geometry were fixed to values determined by Bagnardi and Amelung (2012), and we inverted only for the normalized pressure change (for $r1$) and opening (for $r2$). A third source of deformation (s) was used to reproduce the displacement generated by the pre-eruptive sill intrusion modeled in Section 4.1, and all parameters were fixed to
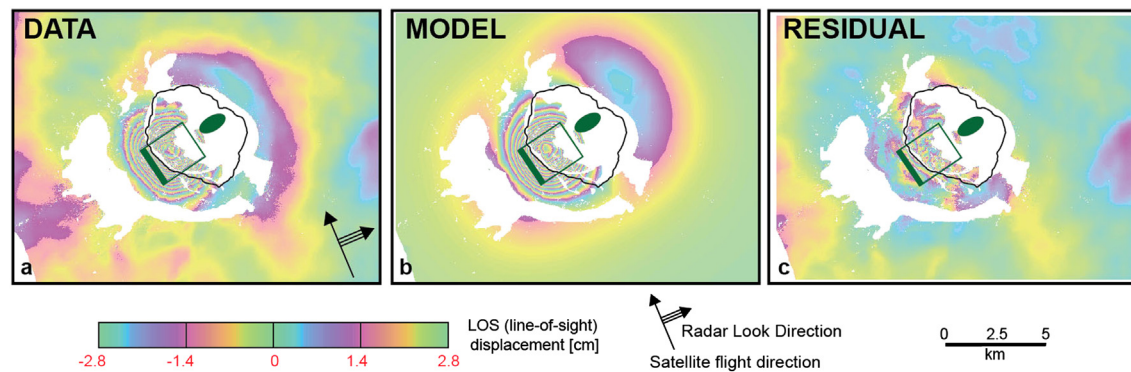
Fig. 4. Modeling of deformation for the April 2009 pre-eruptive sill intrusion. Comparison between (a) measured, (b) modeled, and (c) residual LOS displacement recorded by an Envisat interferogram (track 61, beam model IS2, ascending, 31/01/2009–10/04/2009). Each fringe (full color cycle) represents 2.8 cm of LOS displacement. The green rectangle outlines the geometry of the best-fitting planar source (sill) while the green ellipse represents the center of the deeper magma reservoir beneath the caldera (modeled as an ellipsoidal cavity at ∼5 km depth). (For interpretation of the references to color in this figure legend, the reader is referred to the web version of this article.)

the values of that best-fitting model. To explain the remaining displacement observed on the southwestern flank of the volcano and to best represent the surface expression of the intrusion feeding the eruptive fissures, we followed a multi-step approach. We first ran several forward models to test different combinations (one or more rectangular dislocation sources) and geometries. A reasonable fit to the observed data can only be achieved by using a minimum of two planar sources with uniform opening, oriented parallel to the eruptive fissures, dipping to the SE, and with a dip angle that becomes progressively more vertical with distance from the summit. Successively, we fixed the orientation, location, and size of these two planar sources ($d1$ and $d2$) to values inferred from the forward models (see Table S2 in Supplementary Material) and inverted for dip angle and source opening. The best fit is obtained for a dip angle of 33° from horizontal for $d1$, which is located closer to the summit, and 50° for $d2$, which is located beneath the flank of the volcano.

A comparison between the observed InSAR data, predicted LOS displacement, and residual is shown in Fig. 5. Our model approximations and assumptions result in significant residual deformation for some areas. A clear overestimation of the predicted deformation is present in both viewing geometries where the sill intrusion (s) and the radial intrusion ($d1$) overlap, suggesting that our model does not do a good job of accounting for the complex geometry of the intrusion in this area. For the ascending pass (Fig. 5(d)–(f)), residual interferometric fringes are also present around the summit as result of an overestimation of the negative LOS displacement (subsidence) in this area, which we modeled as deflation of both magma reservoirs. It is probable that the simple geometry of $r1$ (prolate spheroid) is not adequate to explain the observed displacement and a more complex geometry is needed. A similar effect is probably responsible for the overestimated subsidence shown by residual fringes south and east of the radial intrusion. Also, the use of analytical solutions for planar sources having dimensions comparable to, or greater than, the source depth can lead to imprecise estimates of the surface deformation. Despite their limitations and the residuals in some areas, however, these models are instructive for interpreting the geometries of the pre-eruptive sill intrusion, as well as the intrusion that fed the eruption.

4.3. New insights into the January–April 1995 eruption

On the basis of our findings for the 2009 eruption, we reexamine the deformation associated with the similar 1995 eruption. As was the case in 2009, the 1995 eruption was also characterized by deformation of the summit plateau. Uplift of a sub-circular area centered near the southern caldera rim is recorded by two independent interferograms, one from the ERS-1/2 satellites (track 412,

descending, 12/09/1992–30/09/1997, analyzed by Jónsson et al., 1999) and one from the JERS-1 satellite that spans a shorter time interval (Fig. 2(a); track 473, descending, 16/10/1993–11/05/1995). Although the quality of the interferometric signal is higher for the JERS-1 image, we only modeled the ERS-1/2 interferogram because of the absence of significant pre- and post-eruptive deformation in that dataset (the JERS-1 interferogram probably records edifice-wide subsidence due to deflation of the deeper magma reservoir beneath the summit caldera).

Our best fit to the observed deformation is obtained using two planar sources (Okada, 1985), one centered beneath the southwestern caldera rim and dipping (34°) toward the center of the volcano, and one parallel to the radial eruptive fissures and gently dipping (25°) to the SE (Fig. 6, remaining source parameters in Table S3 – Supplementary Material). The geometry and location of the latter source are similar to that of Jónnson et al. (1999), who did not model the remaining deformation at the summit because of decorrelation of the interferometric signal in that area (possibly caused by their use of a different DEM to remove the topographic contribution to the interferometric phase). The deformation model for the 1995 radial eruption therefore strongly resembles that for the 2009 radial eruption, with a shallowly dipping dike on the flank and an inward-dipping sill beneath the summit plateau.

5. Discussion

5.1. Geometry and origin of subvolcanic intrusions

Our deformation modeling, together with inferences from previous studies (Chadwick et al., 2011; Jónsson et al., 1999), reveals the surprising result that, despite their radically different orientations, the 1995 and 2009 radial and the 2005 circumferential eruptions at Fernandina were all fed by shallowly dipping sill intrusions that initiated from, or just beneath, the ∼1-km b.s.l. magma reservoir. In 2005, the intrusion curved to become a steeply dipping dike as it rose toward the surface and erupted as a circumferential fissure near the caldera margin (Fig. 7(a)). This rotation can perhaps be explained by mechanical models indicating that when sills reach a length-to-depth ratio of the order of unity, they are likely to interact with the free surface and rise to shallower levels (Fialko, 2001). In 1995 and 2009, however, the intrusions twisted about an axis oriented radial to the caldera as they propagated toward the flank of the volcano (Fig. 7(b)), becoming shallow-dipping dikes by the time they intersected the surface to feed eruptions from radial fissures. These two radial fissure eruptions were apparently fed by magmatic intrusions with nearly identical geometries but slightly different orientation (directed SSW in 1995 and SW in 2009).
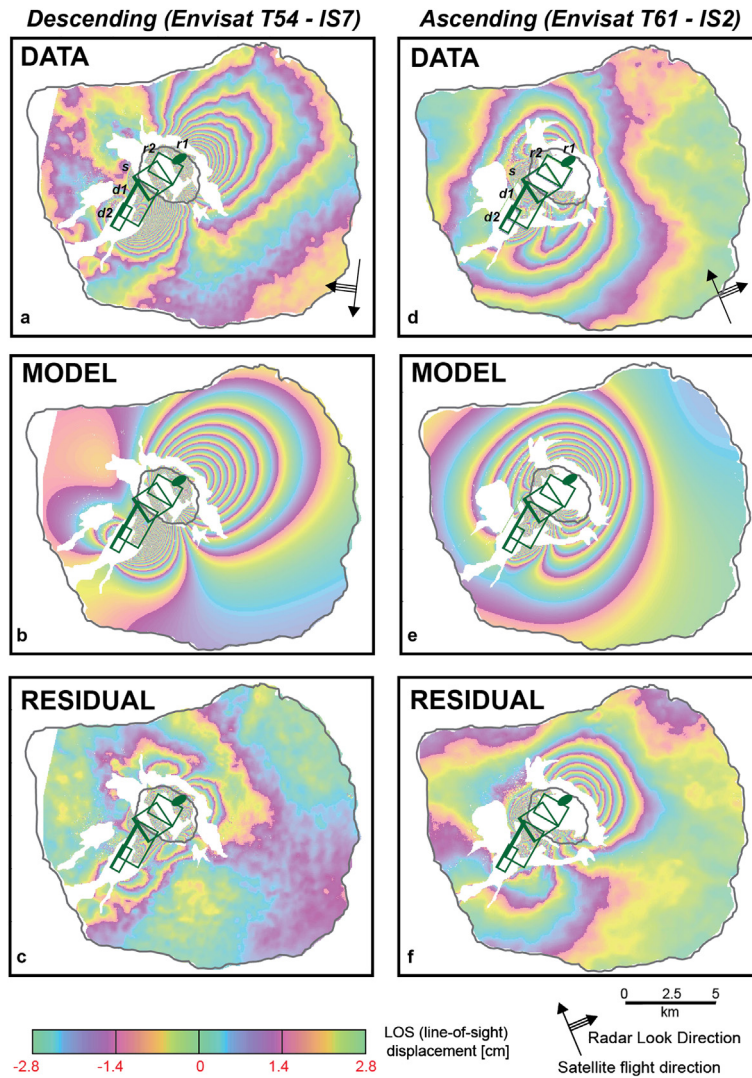
Fig. 5. Modeling of deformation for the April 2009 eruption. Comparison between ((a) and (d)) measured, ((b) and (e)) modeled and ((c) and (f)) residual LOS displacements recorded by two Envisat interferograms (Desc. – 30/01/2009–15/05/2009; Asc. – 31/01/2009–16/15/2009). Each fringe (full color cycle) represents 2.8 cm of LOS displacement. The green ellipse represents the center of the deeper deflation source (r1), and the green rectangles outline the geometries of the planar source models (r2, s, d1 and d2). (For interpretation of the references to color in this figure legend, the reader is referred to the web version of this article.)
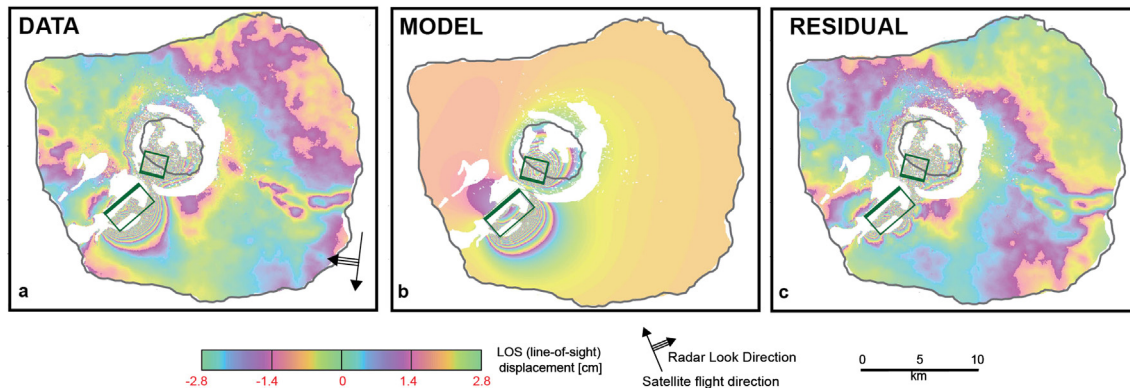

Fig. 6. Modeling of deformation for the January–April 1995 eruption. Comparison between (a) measured, (b) modeled and (c) residual LOS displacement recorded by the ERS-1/2 interferogram (12/09/1992–30/09/1997). Each fringe (full color cycle) represents 2.8 cm of LOS displacement. The green rectangles outline the geometry of the planar source models. (For interpretation of the references to color in this figure legend, the reader is referred to the web version of this article.)

A transition from a sill-like intrusion to a radially aligned dike at some distance from the reservoir is supported by numerical models of interactions between the magma reservoir and volcanic edifice (Hurwitz et al., 2009). Furthermore, the submarine morphology of Fernandina suggests that intrusions that propagate more than ∼10 km beneath the flanks of the volcano may eventually twist into subvertical orientations. Three linear volcanic ridges are present below sea level on the western side of the island
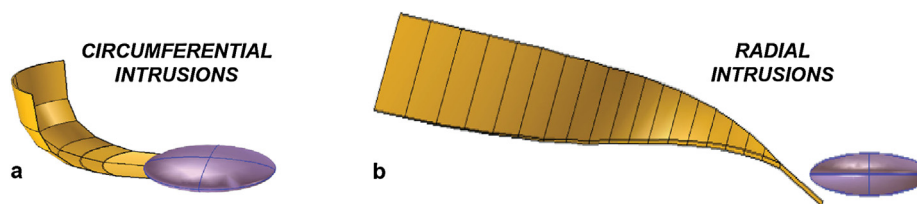
Fig. 7. Three-dimensional representation of circumferential (a) and radial (b) intrusions; in purple the ∼1-km-depth magma reservoir, in yellow the intrusions feeding fissure eruptions (circumferential intrusions as in Chadwick et al., 2011). (For interpretation of the references to color in this figure legend, the reader is referred to the web version of this article.)

(Fig. 1(a)), ∼13–14 km from the summit, and could represent volcanic rift zones similar to those of Hawai'i (Geist et al., 2006b). By analogy, these rift zones are probably underlain by subvertical dikes, leading us to propose that a complete 90-degree twist, from subhorizontal to subvertical, is possible only if the intrusion propagates far enough from the summit.

Although slightly inclined sills initiated both radial and circumferential eruptions, modeling results suggest that they may originate at different depths. In 2005, a subhorizontal intrusion propagated from a modeled depth of ∼1 km b.s.l. (Chadwick et al., 2011), which coincides with the top of the shallower magma reservoir (inferred from independent data; e.g., Bagnardi and Amelung, 2012; Chadwick et al., 2011). Sill intrusions in 1995 and 2009, however, were modeled to have originated at ∼2.0 and ∼2.3 km b.s.l. respectively (the difference between the two is probably not significant). Support for these findings can be found in the strikingly different petrologic signatures between the lavas erupted in 1995 and 2005, with the former bearing abundant phenocrysts (plagioclase, clinopyroxene, and olivine) and the latter containing only few small phenocrysts grown from the liquid shortly before eruption. To explain this difference, Chadwick et al. (2011) proposed that the intrusion that fed the 1995 eruption eroded plagioclase-rich crystal mush from the margin of the magma reservoir. In contrast, the 2005 dike propagated from the top of the reservoir and did not encounter the deeper mush zone.

On a broader scale, the characteristic pattern of radial and circumferential fissures shown at Fernandina is evident to varying degrees at all volcanoes in the western Galápagos (Chadwick and Howard, 1991), suggesting that the processes controlling intrusive and eruptive dynamics at Fernandina are common to all the edifices in the archipelago. Similar patterns of eruptive fissures are also present outside the Galápagos, including many seamounts (Batiza et al., 1984; Simkin, 1972), other ocean islands (Jaggar, 1931; MacDonald, 1948), and even on Mars (Montési, 2001). Our results and interpretations are consistent with the numerical modeling of Grosfils (2007), who demonstrated that elastic models of magma-reservoir rupture cannot produce laterally propagating, subvertical dikes under any geological and geometrical conditions. Feeding radial fissures in the Galápagos and elsewhere via rotated subhorizontal sills, therefore, is consistent with modeled stress conditions within a volcanic edifice. Magma transport by mean of subhorizontal sills has also been recognized as an important element controlling the growth and evolution of shield volcanoes of the Canary Islands (Staudigel et al., 1986; Ancochea et al., 2008) and La Réunion Island (Famin and Michon, 2010). Our model for magma transport at the Galápagos may therefore be broadly applicable to other subaerial, submarine, and extraterrestrial volcanoes, and provides an alternative to interpretations based on the example of Hawai'i.

5.2. Type and location of the next Fernandina eruption

Our observations and models of Fernandina may also be used to forecast the location and orientation of future eruptive fissures
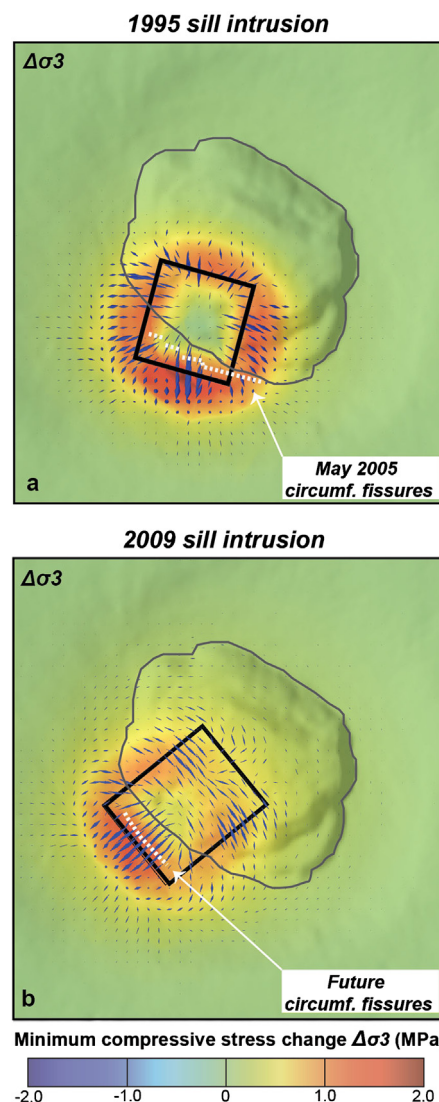

Fig. 8. Models of stress change due to sill intrusions. Magnitude (background) and orientation (blue arrowheads) of the changes in the minimum compressive stress after the (a) 1995 and (b) 2009 sill intrusions (black rectangles) at 0 km depth (sea level). Arrowhead length is proportional to change in σ_3 and to its plunge (maximum when horizontal). White-dashed lines mark the location of the May 2005 eruptive fissures in part (a) and of the forecasted location of future fissures in part (b). Based on this example and the stress change due to the 2009 sill, we forecast that the next eruption will be from a circumferential fissure within the area uplifted by the 2009 sill intrusion. (For interpretation of the references to color in this figure legend, the reader is referred to the web version of this article.)

(e.g., Walter, 2008). Previous studies (Chadwick and Dieterich, 1995; Chadwick et al., 2011) have suggested a general feedback between radial and circumferential fissure eruptions because the stresses created by a radial dike would favor future intrusions with a circumferential orientation, and vice versa. This is consis-

tent with the recent alternation between fissure eruption trends (circumferential in 1982, radial in 1995, circumferential in 2005, and radial in 2009, all in the same sector of the volcano).

Modeling of stress changes produced by the intrusion of a sill beneath the summit plateau in 1995 indicates a positive change of the least compressive stress in the crust, σ_3, beneath the area in which the 2005 circumferential eruptive fissures opened (Fig. 8(a)). This change is directed radially with respect to the summit, favoring the intrusion of a circumferential dike in this area. We therefore suggest that the orientation and location of the 2005 eruptive fissures was controlled by the stress perturbation imposed by the sill intrusion that was emplaced at the start of the 1995 eruption. Based on this example, the model of deformation during the April 2009 eruption could be used to forecast the type and location of future eruptive fissures. The stress change generated by the 2009 pre-eruptive sill intrusion indicates that the greatest positive change in σ_3 occurred along the SW rim of the summit caldera (Fig. 8(b)). We therefore project that the next eruption at Fernandina will be from circumferential fissures within the area uplifted by the 2009 sill intrusion, near the caldera rim and northwest of the 2005 eruption site.

6. Conclusions

Results from the analysis and modeling of space-geodetic data spanning both radial and circumferential fissure eruptions at Fernandina volcano have led us to a new interpretation of the dynamics of magma migration and internal growth at Galápagos volcanoes. Contrary to the assumption of magma transport through vertical dikes, we have demonstrated that both orientations of eruptive fissures are initiated by the intrusion of subhorizontal sills. These intrusions curve upward to become steeply dipping dikes when feeding circumferential fissures near the caldera margin or twist about a radially oriented axis to feed fissure eruptions on the flanks of the volcano. While the mechanism for the stress field that causes these unique geometries remains ambiguous, our model for the development of intrusions that feed eruptive activity at Fernandina does provide insights into the subsurface structure of Galápagos and similar volcanoes, as well as the process by which they grow.

The intrusion of subhorizontal sills during the initial stages of a radial fissure eruption could explain the apparent alternation between eruption types, with circumferential eruptions occurring as a consequence of perturbations in the stress field generated by the preceding radial fissure eruption. Such a model provides a means of forecasting the style and location of future eruptions, although their timing cannot be predicted at this point. The 2005 circumferential eruption occurred in the area that experienced the most uplift in 1995 due to emplacement of the sill that fed that radial fissure eruption. By analogy, and with the support of stress change modeling of the 2009 pre-eruptive sill intrusion, we anticipate that the next eruption at Fernandina will probably occur from circumferential fissures opening within the area uplifted in 2009.

Acknowledgements

Appendix A. Supplementary material

Supplementary material related to this article can be found online at http://dx.doi.org/10.1016/j.epsl.2013.07.016.

References

Amelung, F., Jónsson, S., Zebker, H., Segall, P., 2000. Widespread uplift and "trapdoor" faulting on Galápagos volcanoes observed with radar interferometry. Nature 407, 993–996.

Ancochea, E., Brändle, J.L., Huertas, M.J., Hernán, F., Herrera, R., 2008. Dike-swarms, key to the reconstruction of major volcanic edifices: The basic dikes of La Gomera (Canary Islands) J. Volcanol. Geotherm. Res. 173, 207–216.

Bagnardi, M., Amelung, F., 2012. Space-geodetic evidence for multiple magma reservoirs and subvolcanic lateral intrusions at Fernandina Volcano, Galápagos Islands. J. Geophys. Res. 117. B10406.

Baker, S., Amelung, F., 2012. Top-down inflation and deflation at the summit of Kīlauea Volcano, Hawai'i observed with InSAR. J. Geophys. Res. 117. B12406.

Batiza, R., Fornari, D.J., Vanko, D.A., Lonsdale, P., 1984. Craters, calderas, and hyaloclastites on young Pacific seamounts. J. Geophys. Res. 89, 8371.

Bistacchi, A., Tibaldi, A., Pasquarè, F., Rust, D., 2012. The association of cone-sheets and radial dykes: Data from the Isle of Skye (UK), numerical modelling, and implications for shallow magma chambers. Earth Planet. Sci. Lett. 339–340, 46–56.

Brooks, B.A., Frazer, L. Neil, 2005. Importance reweighting reduces dependence on temperature in Gibbs samplers: An application to the coseismic geodetic inverse problem. Geophys. J. Int. 161, 12–20.

Chadwick, W.W., Dieterich, J.H., 1995. Mechanical modeling of circumferential and radial dike intrusion on Galapagos volcanoes. J. Volcanol. Geotherm. Res. 66, 37–52.

Chadwick, W.W., Howard, K.A., 1991. The pattern of circumferential and radial eruptive fissures on the volcanoes of Fernandina and Isabela islands, Galapagos. Bull. Volcanol. 53, 259–275.

Chadwick, W.W., Jónsson, S., Geist, D.J., Poland, M., Johnson, D.J., Batt, S., Harpp, K.S., Ruiz, A., 2011. The May 2005 eruption of Fernandina volcano, Galápagos: The first circumferential dike intrusion observed by GPS and InSAR. Bull. Volcanol. 73, 679–697.

Chen, C.W., Zebker, H.A., 2001. Two-dimensional phase unwrapping with use of statistical models for cost functions in nonlinear optimization. J. Opt. Soc. Am. 18, 338–351.

Dieterich, J.H., 1988. Growth and persistence of Hawaiian volcanic rift zones. J. Geophys. Res. 93, 4258.

Famin, V., Michon, L., 2010. Volcano destabilization by magma injections in a detachment. Geology 38, 219–222.

Farr, T.G., Rosen, P.A., Caro, E., Crippen, R., Duren, R., Hensley, S., Kobrick, M., Paller, M., Rodriguez, E., Roth, L., Seal, D., Shaffer, S., Shimada, J., Umland, J., Werner, M., Oskin, M., Burbank, D., Alsdorf, D., 2007. The shuttle radar topography mission. Rev. Geophys. 45. RG2004.

Fialko, Y., 2001. On origin of near-axis volcanism and faulting at fast spreading mid-ocean ridges. Earth Planet. Sci. Lett. 190, 31–39.

Fiske, R.S., Jackson, E.D., 1972. Orientation and growth of Hawaiian volcanic rifts: The effect of regional structure and gravitational stresses. Proc. R. Soc., Math. Phys. Eng. Sci. 329, 299–326.

Geist, D., Chadwick, W., Johnson, D., 2006a. Results from new GPS and gravity monitoring networks at Fernandina and Sierra Negra volcanoes, Galápagos, 2000–2002. J. Volcanol. Geotherm. Res. 150, 79–97.

Geist, D.J., Fornari, D.J., Kurz, M.D., Harpp, K.S., Adam Soule, S., Perfit, M.R., Koleszar, A.M., 2006b. Submarine Fernandina: Magmatism at the leading edge of the Galápagos hot spot. Geochem. Geophys. Geosyst. 7. Q12007.

Grosfils, E.B., 2007. Magma reservoir failure on the terrestrial planets: Assessing the importance of gravitational loading in simple elastic models. J. Volcanol. Geotherm. Res. 166, 47–75.

Hurwitz, D.M., Long, S.M., Grosfils, E.B., 2009. The characteristics of magma reservoir failure beneath a volcanic edifice. J. Volcanol. Geotherm. Res. 188, 379–394.

Jaggar, T.A., 1931. Geology and geography of Niuafo'ou volcano. Volc. Lett. 318, 1–3.

Jónsson, S., 2009. Stress interaction between magma accumulation and trapdoor faulting on Sierra Negra volcano, Galápagos. Tectonophysics 471, 36–44.

Jónsson, S., Zebker, H., Cervelli, P., Segall, P., Garbeil, H., Mouginis-Mark, P., Rowland, S., 1999. A shallow-dipping dike fed the 1995 flank eruption at Fernandina Volcano, Galápagos, observed by satellite radar interferometry. Geophys. Res. Lett. 26, 1077–1080.

Jónsson, S., Zebker, H., Segall, P., Amelung, F., 2002. Fault slip distribution of the 1999 Mw 7.1 Hector Mine, California, Earthquake, estimated from satellite radar and GPS measurements. Bull. Seismol. Soc. Am. 92, 1377–1389.

Kauahikaua, J., Poland, M., 2012. One hundred years of volcano monitoring in Hawaii. Eos Trans. AGU 93, 29.

Macdonald, G.A., 1948. Notes on Niuafo'ou. Am. J. Sci. 246, 65–77.

Montési, L.G.J., 2001. Concentric dikes on the flanks of Pavonis Mons: Implications for the evolution of martian shield volcanoes and mantle plumes. In: Ernst, R.E., Buchan, K.L. (Eds.), Mantle Plumes: Their Identification through Time. Boulder, Colorado. In: Spec. Pap., Geol. Soc. Am., vol. 352, pp. 165–181.

Muller, J.R., Ito, G., Martel, S.J., 2001. Effects of volcano loading on dike propagation in an elastic half-space. J. Geophys. Res. 106 (B6), 11101–11113.

Munro, D.C., Rowland, S.K., 1996. Caldera morphology in the western Galápagos and implications for volcano eruptive behavior and mechanisms of caldera formation. J. Volcanol. Geotherm. Res. 72, 85–100.

Nakamura, K., 1980. Why do long rift zones develop in Hawaiian volcanoes: A possible role for thick oceanic sediments. Bull. Volcanol. Soc. Japan Ser. 2 25 (4), 255–269 (in Japanese); English translation in: Proceedings of the International Symposium on the Activity of Oceanic Volcanoes. In: Ser. Cienc. Nat., vol. 3. Universidade dos Azores, Ponta Delgada, 1982, pp. 59–73.

Naumann, T., Geist, D., Kurz, M., 2002. Petrology and geochemistry of Volcán Cerro Azul: Petrologic diversity among the western Galápagos volcanoes. J. Petrol. 43, 859–883.

Nordlie, B.E., 1973. Morphology and structure of the western Galapagos volcanoes and a model for their origin. Geol. Soc. Am. Bull. 84, 2931–2956.

Okada, Y., 1985. Surface deformation due to shear and tensile faults in a half-space. Bull. Seismol. Soc. Am. 75 (4), 1135–1154.

Pollard, D.D., Delaney, P.T., Duffield, W.A., Endo, E.T., Okamura, A.T., 1983. Surface deformation in volcanic rift zones. Tectonophysics 94, 541–584.

Rosen, P.A., Hensley, S., Peltzer, G., Simons, M., 2004. Updated repeat orbit interferometry package released. Eos Trans. AGU 85, 47.

Rowland, S., Munro, D., 1992. The caldera of volcan Fernandina: A remote sensing study of its structure and recent activity. Bull. Volcanol., 97–109.

Rubin, A.M., Pollard, D.D., 1987. Origins of blade-like dikes in volcanic rift zones. In: U.S. Geol. Surv. Prof. Pap., vol. 1350, pp. 1449–1470.

Simkin, T., 1972. Origin of some flat-topped volcanoes and guyots. Mem. Geol. Soc. Amer. 132, 183–193.

Simkin, T., 1984. Geology of Galapagos Islands. In: Perry, R. (Ed.), Key Environments: Galapagos. Pergamon, Oxford, pp. 16–41.

Staudigel, H., Feraud, G., Giannerini, G., 1986. The history of intrusive activity on the island of La Palma (Canary Islands). J. Volcanol. Geotherm. Res. 27, 299–322.

Tilling, R.I., Dvorak, J.J., 1993. Anatomy of a basaltic volcano. Nature 363, 125–133.

Walker, G.P.L., 1987. Volcanism in Hawaii. In: U.S. Geol. Surv. Prof. Pap., vol. 2, p. 961.

Walter, T.R., 2008. Facilitating dike intrusions into ring-faults. In: Developments in Volcanology. Elsevier, pp. 352–374.

Williams, C.A., Wadge, G., 1998. The effects of topography on magma chamber deformation models: Application to Mt. Etna and radar interferometry. Geophys. Res. Lett. 25, 1549–1552.

Yang, X.-M., Davis, P.M., Dieterich, J.H., 1988. Deformation from inflation of a dipping finite prolate spheroid in an elastic half-space as a model for volcanic stressing. J. Geophys. Res. 93, 4249.